# Supporting Information

## Structurally controllable Cd(II)-based luminescent metal-organic frameworks for efficient detection of antibiotics in water

Ning Xu, Yulong Zhou, Yexin Shen, Rui Li, Qinghua Zhang and Xiandong Zhu*

*Anhui Province Key Laboratory of Functional Coordinated Complexes for Materials Chemistry and Application, School of Chemical and Environmental Engineering, Anhui Polytechnic University, Wuhu, Anhui 241000, P.R. China.*

E-mail: zhuxd@ahpu.edu.cn

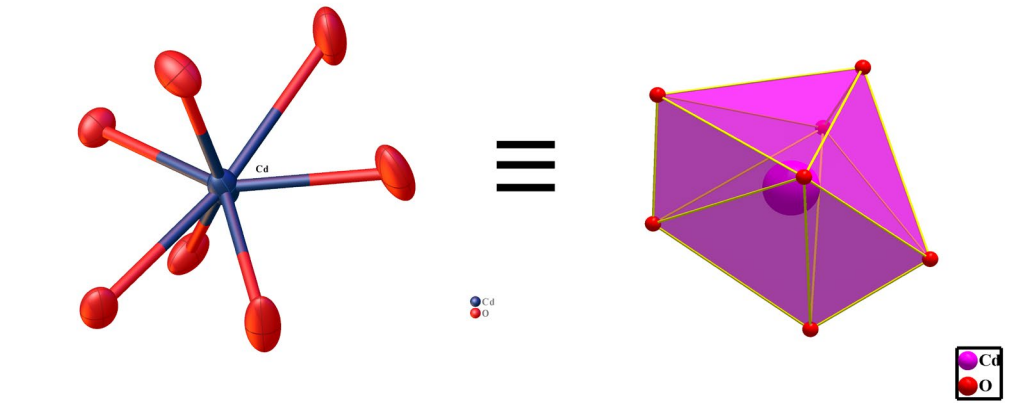


**Fig. S1.** The coordination mode of $Cd^{2+}$ ions in **FCS-8**.

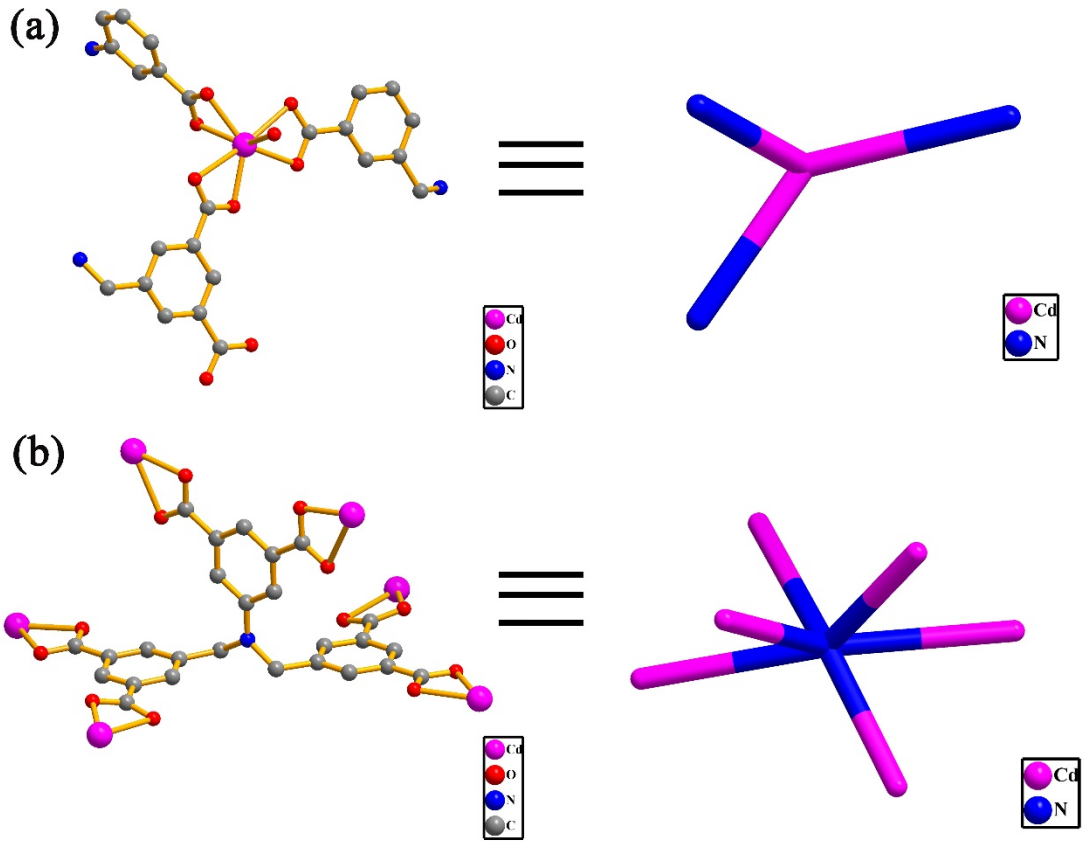


**Fig. S2.** (a) $Cd^{2+}$ ions as 3-c nodes and (b) $bmipia^{6-}$ ligand as 6-c nodes in **FCS-8**.

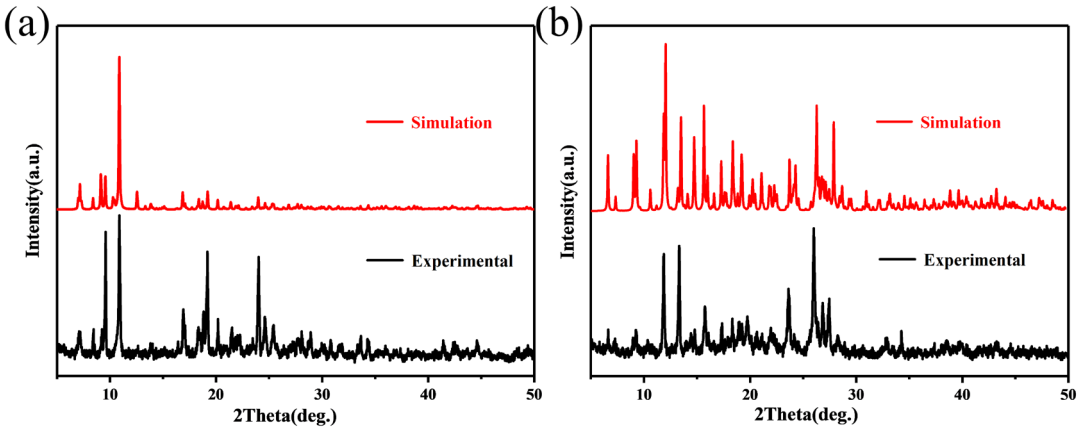


**Fig. S3.** The powder X-ray diffraction patterns of **FCS-7** (a) and **FCS-8** (b).

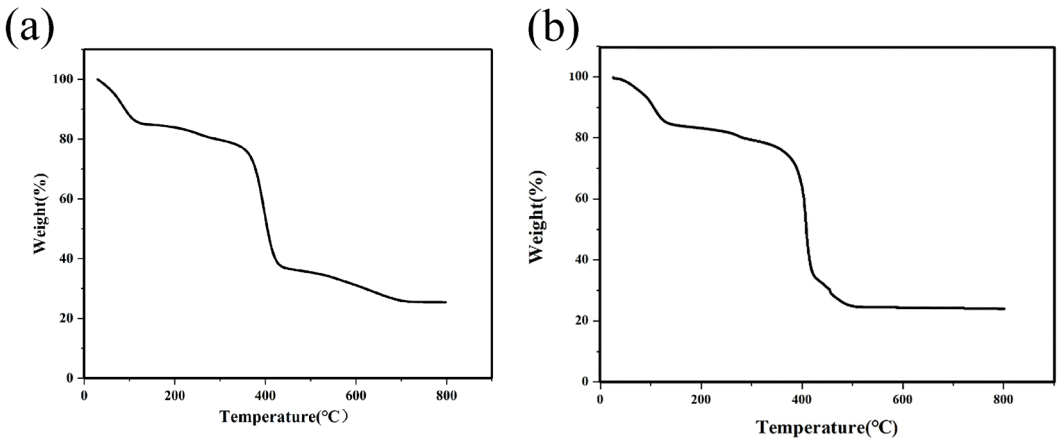


**Fig. S4.** The thermogravimetric analyses for **FCS-7** (a) and **FCS-8** (b).

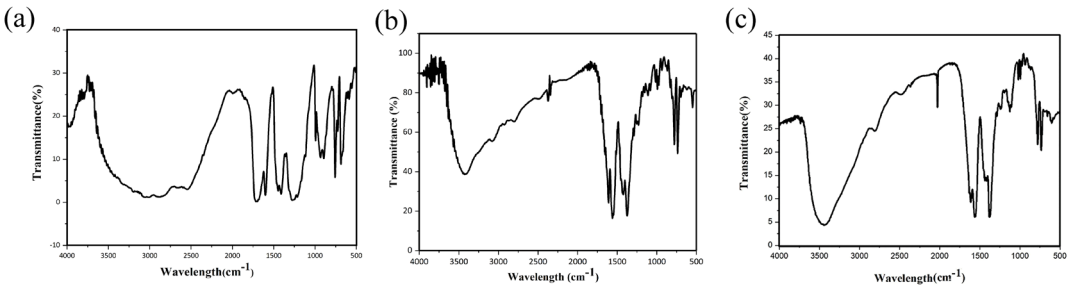


**Fig. S5.** The infrared spectra of **L** (a), **FCS-7** (b) and **FCS-8** (c).

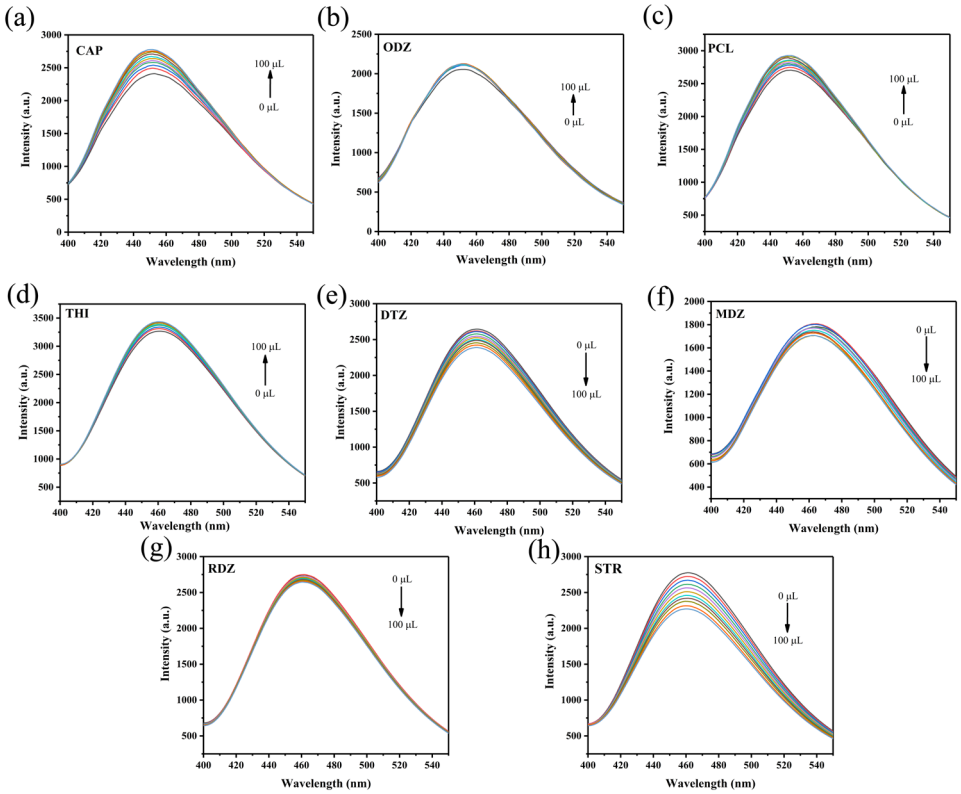


**Fig. S6.** The fluorescence titration of **FCS-7** with the gradual addition of CAP(a), ODZ(b), PCL(c), THI(d), DTZ(e), MDZ(f), RDZ(g) and STR(h).

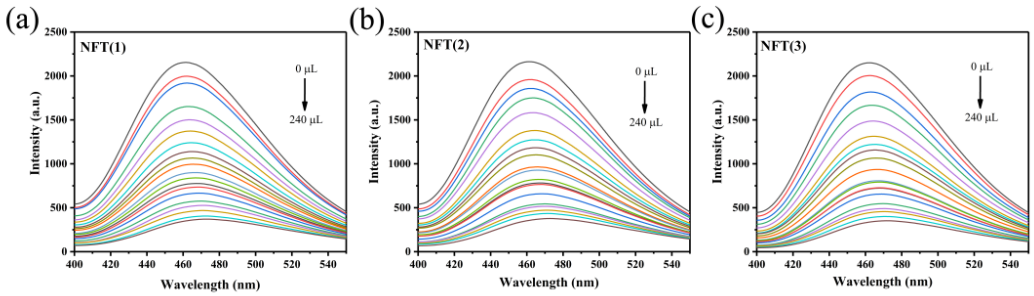


**Fig. S7.** The three fluorescence titrations of **FCS-7** with gradual addition of NFT.

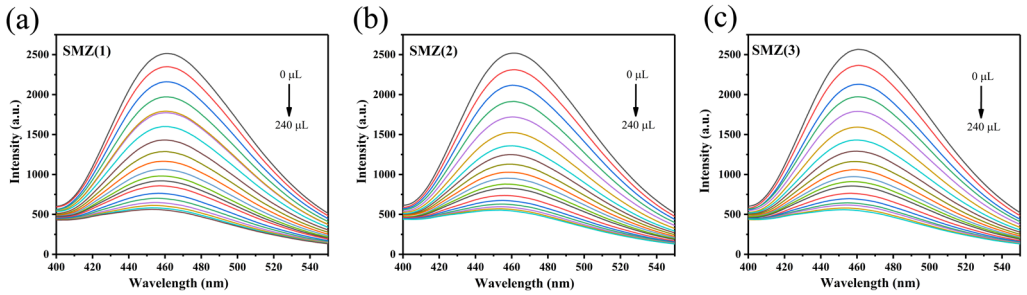


**Fig. S8.** The three fluorescence titrations of **FCS-7** with gradual addition of SMZ.

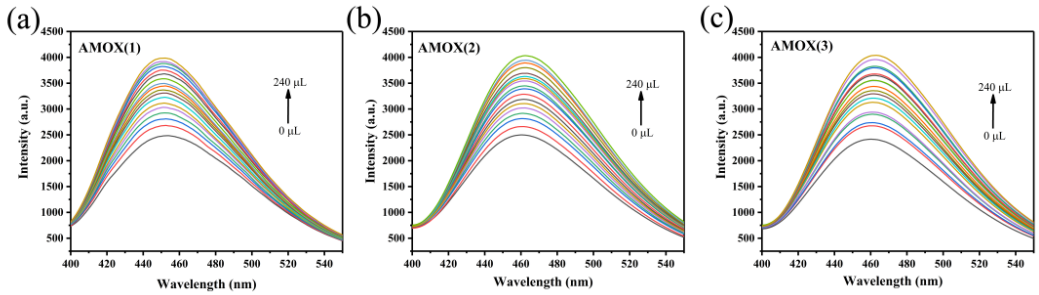


**Fig. S9.** The three fluorescence titrations of **FCS-7** with gradual addition of AMOX.

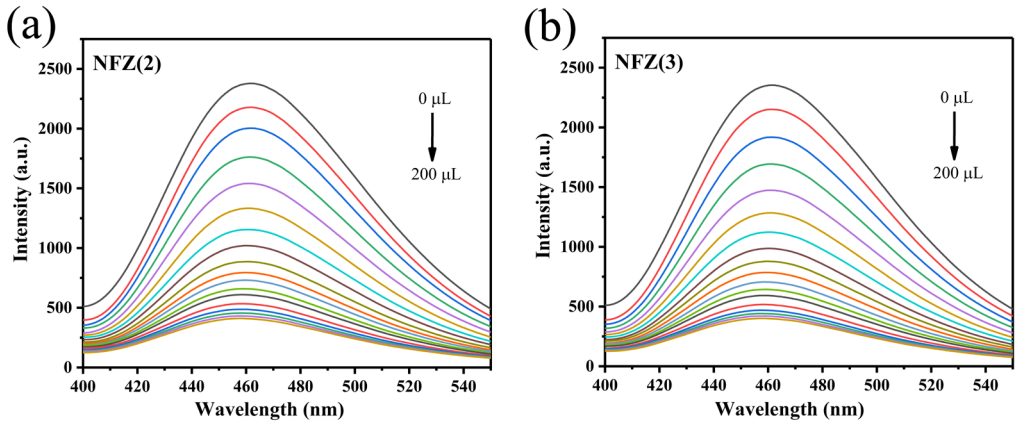


**Fig. S10.** The two fluorescence titrations of **FCS-7** with gradual addition of NFZ.

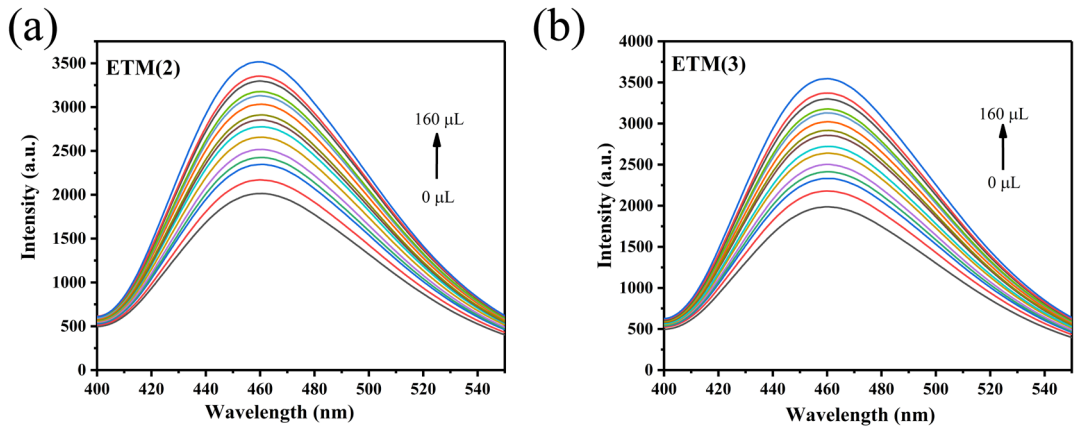


**Fig. S11.** The two fluorescence titrations of **FCS-7** with gradual addition of ETM.

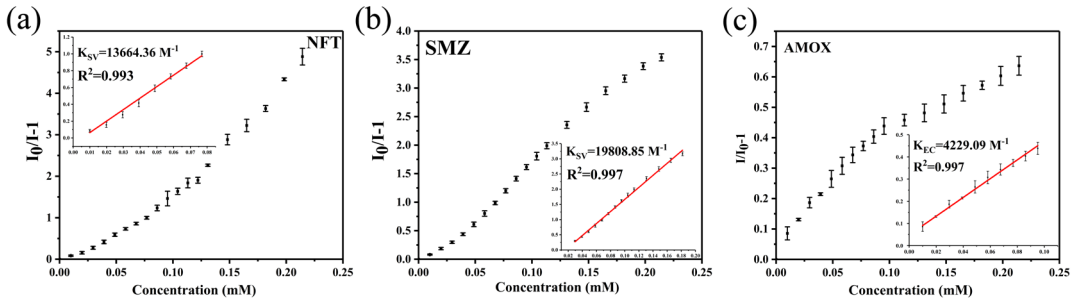


**Fig. S12.** Correlation curves of **FCS-7** calculated by using the Stern–Volmer equation for the detection of NFT(a), SMZ(b) and AMOX(c). Inset: linear fitting plots in the low concentration region.

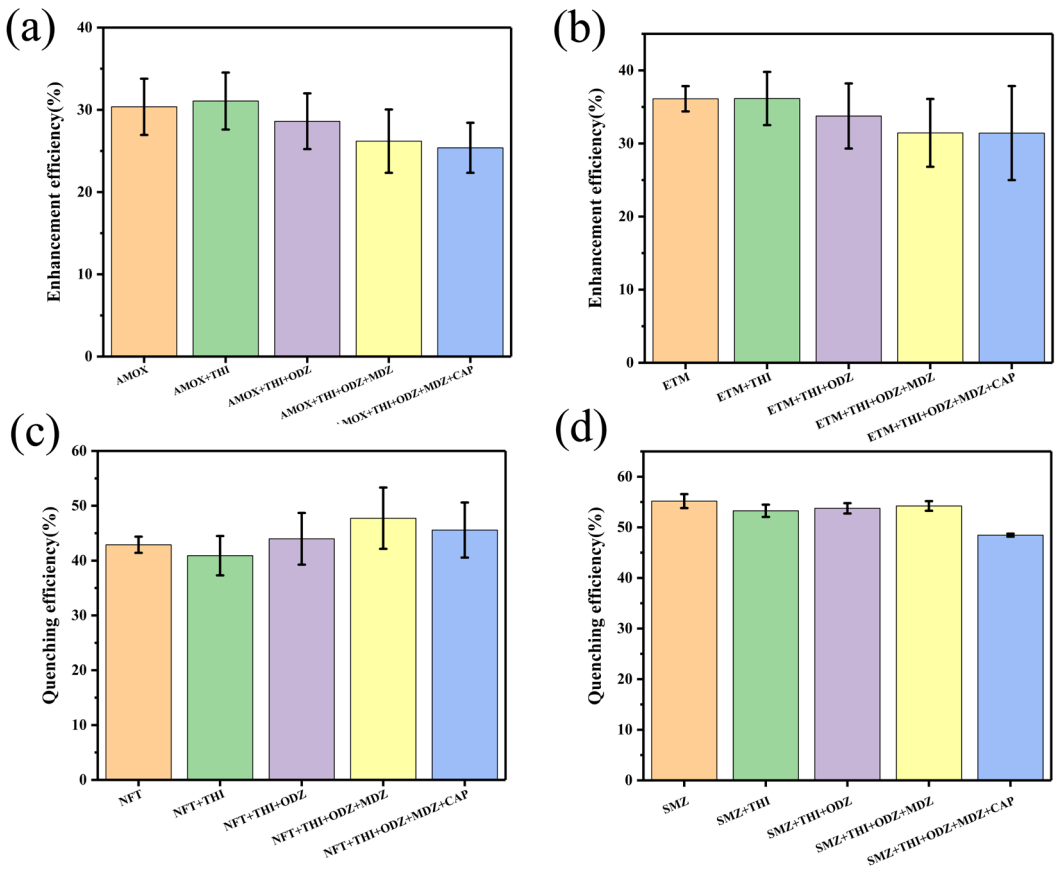


**Fig. S13.** The anti-interference ability of **FCS-7** toward AMOX(a), ETM(b), NFT(c) and SMZ(d) in the presence of various kinds of interfering antibiotics.

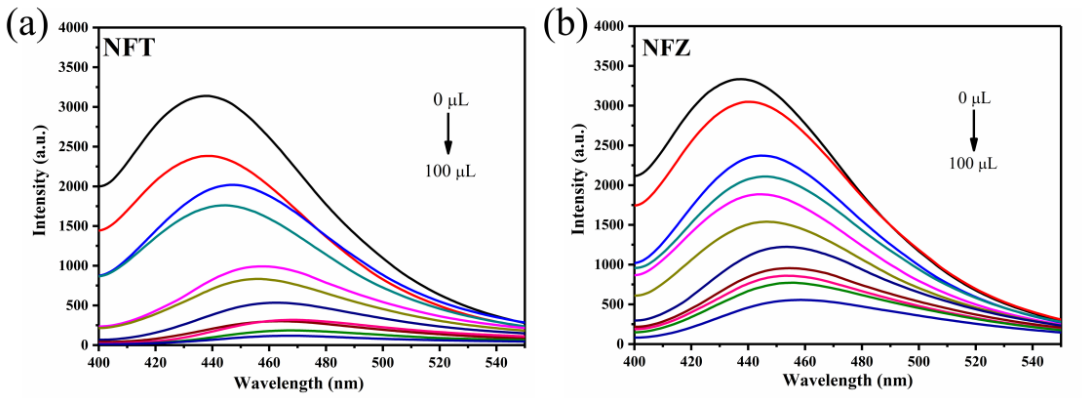


**Fig. S14.** The fluorescence titration of **FCS-8** with the gradual addition of (a) NFT and (b) NFZ.

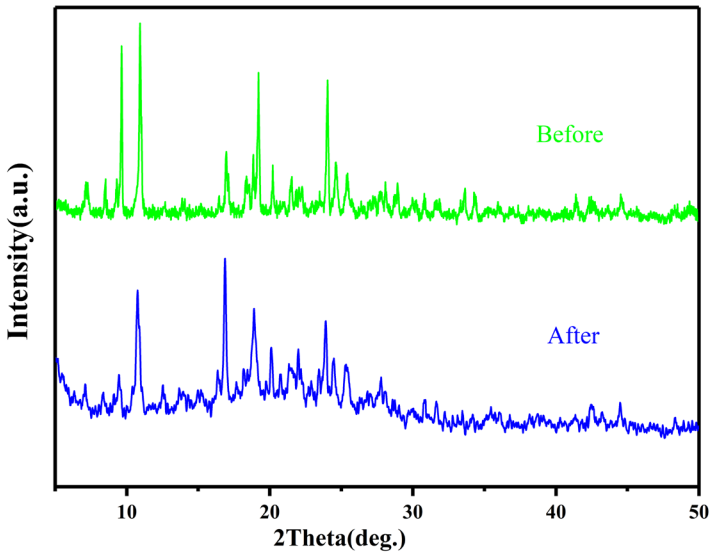


**Fig. S15.** The Powder X-ray diffraction patterns of **FCS-7** before and after the fluorescence quenching experiment induced by NFZ.

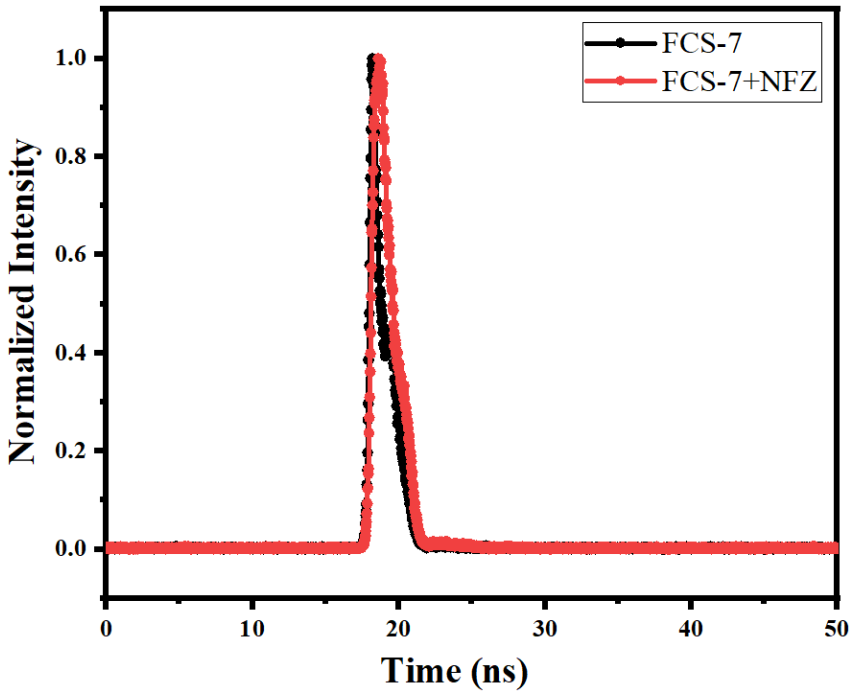


**Fig. S16.** Time-resolved fluorescence decay of **FCS-7** before (black) and after (red) the addition of NFZ.

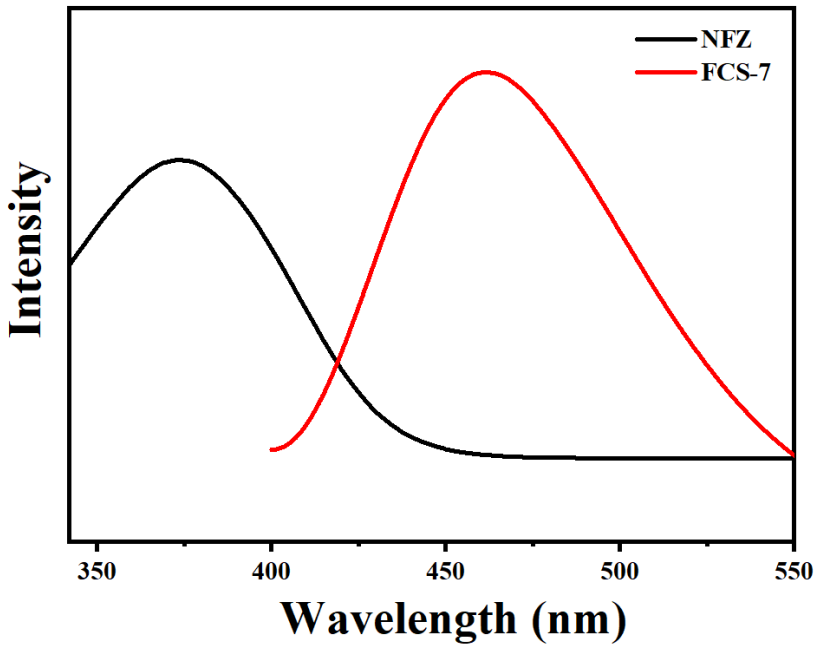


**Fig. S17.** UV-vis absorption spectra of NFZ and the normalized emission spectra of **FCS-7** in water.

**Table S1.** Crystallographic data and structure refinement parameters for **FCS-7** and **FCS-8**.

| Compoundes | FCS-7 | FCS-8 |
|---|---|---|
| **Empirical formula** | $C_{52}H_{46}O_{44}N_2Cd_4Na_2$ | $C_{52}H_{66}O_{42}N_2Cd_4$ |
| **Formula weight** | 1897.08 | 1840.66 |
| **Temperature** | 273.15 K | 100.15 K |
| **Crystal system** | monoclinic | orthorhombic |
| **Space group** | C2/c | Ccce |
| **a (Å)** | 18.813(6) | 20.2245(10) |
| **b (Å)** | 17.151(5) | 24.9058(10) |
| **c (Å)** | 25.366(8) | 17.2568(8) |
| ***α*** **(°)** | 90 | 90.00 |
| ***β*** **(°)** | 104.339(13) | 90.00 |
| ***γ*** **(°)** | 90 | 90.00 |
| **Z** | 4 | 4 |
| $D_c$**/(g cm$^{-3}$)** | 1.589 | 1.407 |
| **F(000)** | 3750.0 | 3680.0 |
| ***θ*** **range (°)** | 3.9 to 55.348 | 5.19 to 60.992 |
| **Reflections collected** | 80239 | 38610 |
| **Data / restraints / parameters** | 9123/2/443 | 6601 / 24 / 281 |
| **Goodness-of-fit on F²** | 1.066 | 1.099 |
| **R1 indices(I > 2 σ (I))** | 0.0517 | 0.0553 |
| **wR₂ indices(all date)** | 0.1672 | 0.1609 |

[a] $R = \sum||F_o|-|F_c||/\sum|F_o|$. [b] $wR(F^2)=[\sum(w(F_o^2-F_c^2)^2/\sum(w(F_o^2)^2]^{1/2}$.

**Table S2.** Comparison of the proposed detection method in this study with other literature.

| Complexes | Objective | LDR | Ksv | LOD | Ref. |
|---|---|---|---|---|---|
| $[Cd(mba)(bpdb)_{0.5}]$ | NFZ | 1-10 μM | 81498 $M^{-1}$ | 0.123 μM | [1] |
| $[Zn(L^1)_{0.5}(L^2)_{0.5}(H_2O)]\cdot DMF$ | NFZ | 0-29.1 μM | 52000 $M^{-1}$ | 19.6 μM | [2] |
| $\{[Cd(L)_{0.5}(bpe)_{0.5}(H_2O)]\cdot x(solv)\}$ | NFZ | 0-90 μM | 35000 $M^{-1}$ | 0.33 μM | [3] |
| $\{[Zn(TTPA)]\cdot 1.5DMA\}_n$ | NFZ | 0-50 μM | 23500 $M^{-1}$ | 6.57 μM | [4] |
| $Zr_6O_6(OH)_2(TDCA)_4(CH_3COO)_2$ | NFZ | 0.7-250.4 μM | -- | 0.25 μM | [5] |
| $[Cd(L_1)(1,4\text{-}NDA)]_n$ | NFZ | 0-100 μM | 3854 $M^{-1}$ | 2.02 μM | [6] |
| ssDNA | NFZ | 1.25-160 ng/mL | -- | 1.13 ng/mL | [7] |
| $WO_3/CuMnO_2$ | NFZ | 0.015-32 μM | -- | 1.19 nM | [8] |
| O-AgNPs | NFZ | 1-500 μM | -- | 1.88 μM | [9] |
| **FCS-7** | NFZ | 3-40 μM | 121170.44 $M^{-1}$ | 92 $\mu g\cdot L^{-1}$ | This work |

**Table S3.** HOMO and LUMO energies for $H_6$bmipia and NFZ calculated by density functional theory (DFT) with B3LYP/6-31+G* basis set.

| Compound | HOMO (eV) | LUMO (eV) | Band Gap (eV) |
|---|---|---|---|
| $H_6$bmipia | -6.2015 | -2.3179 | 3.8836 |
| NFZ | -6.6963 | -3.2462 | 3.61022 |

## References


1. K. Wang, X. Bai, X. Zhao, Y. Dong, R. Zhao, J. Zhou, H. Yu, L. Li, H. Tang and Y. Ma, *J. Mol. Struct.*, 2023, **1292**, 136114.
2. J.-M. Liu, Y.-B. Ren, H.-Y. Xu, L.-J. Li, Y.-J. Mu and J.-L. Du, *Inorg. Chim. Acta.*, 2021, **527**, 120583.
3. M. Lei, F. Ge, S. Ren, X. Gao and H. Zheng, *Sep. Purif. Technol.*, 2022, **286**, 120433.
4. Z. Long Ma, M. Chen Wang, L. Tian and L. Cheng, *Inorg. Chim. Acta.*, 2021, **526**, 120513.
5. H. Wang, X. Bo, M. Zhou and L. Guo, *Anal. Chim. Acta*, 2020, **1109**, 1-8.
6. M.-Y. Wen, L. Fu and G.-Y. Dong, *J. Mol. Struct.*, 2023, **1285**, 135488.
7. X. Wen, X. Yan, X. Zheng, Q. Kou, L. Yang, J. Tang, X. Chen, Y. Xie and T. Le, *Anal. Chim. Acta*, 2023, **1252**, 341044.
8. S. Velmurugan, T. C.-K. Yang, J. Ching Juan and J.-N. Chen, *J. Colloid Interface Sci.*, 2021, **596**, 108-118.
9. S. W. Ahmed, H. Anwar, Shama, A. Siddiqui, M. R. Shah, A. Ahmed and S. A. Ali, *Sens. Actuators, B*, 2018, **256**, 429-439.